DYNAMICS OF TWO-DIMENSIONAL CANTILEVERED THIN FLEXIBLE PLATES IN AXIAL FLOW: ENERGY TRANSFER AND THE DESIGN OF A FLUTTER-MILL

Liaosha Tang

University of Toronto Institute for Aerospace Studies, Toronto, Canada

Michael P. Païdoussis

Department of Mechanical Engineering, McGill University, Montreal, Canada

Jin Jiang

School of Power and Mechanical Engineering, Wuhan University, Wuhan, P.R.China

ABSTRACT

Cantilevered flexible plates in axial flow loses stability at sufficiently high flow velocity. Once the stability threshold is exceeded, flutter takes place, and energy is continuously pumped into the plate from the surrounding fluid flow for sustaining the flutter motion. This kind of self-induced vibration can be utilized to extract energy from the fluid flow. This paper first studies the energy transfer between the fluid flow and the plate. Then, based on the energy analysis of the fluid-structure interaction system, a new concept of energy-harvesting, the flutter-mill, is proposed to utilize these flutter motions to generate electrical power.

1. INTRODUCTION

Flutter is not always an unfavourable phenomenon; it can be utilized to do useful work, for example, for the generation of electricity. The oil crisis in the mid-1970s encouraged the pursuit of alternative sources of energy; many designs of *unconventional* energy-harvesting devices utilizing the flutter motions of airfoils/wings came into being at that time. The idea of an oscillating-wing windmill (the so-called wingmill) was proposed by McKinney and DeLaurier (1981). The studies on the wingmill continued (Matsumoto et al., 2006), and a patent (Lee, 2004) was recently granted.

The dynamics of cantilevered thin flexible plates in subsonic axial flow has recently been reviewed by Tang and Païdoussis (2007) in a systematic manner. The two-dimensional plate is modelled as a beam with an inextensible centre-line, and an unsteady lumped vortex model is used to calculate the pressure difference across the laterally oscillating plate. The analysis of

the system dynamics is carried out in the time-domain. The system loses stability by flutter at sufficiently high flow velocity, and both the instability threshold, as a function of the system parameters, and the post-critical behaviour of the system have been extensively studied. The present paper investigates the energy transfer between the plate and the surrounding fluid flow. Based on the energy analysis, the design of a new energy-harvesting device, the "flutter-mill", is proposed. In the light of the dynamics of the system, key system parameters of the flutter-mill can be determined. Moreover, the performance of the flutter-mill is preliminarily evaluated and compared to a real horizontal axial wind turbine (HAWT) (Burton et al., 2001).

2. THE FLUID-ELASTIC MODEL

A schematic diagram of a cantilevered flexible plate in axial flow is shown in Fig. 1. The geometrical characteristics of the rectangular homogeneous plate are the length of the flexible section L, width B and thickness h; $B \to \infty$ and $h \ll L$ for a two-dimensional thin plate. Normally, there is a rigid segment of length L_0 as part of the clamping arrangement at the upstream end. The other physical parameters of the system are: the plate material density ρ_P and bending stiffness $D = Eh^3/\sqrt{12(1 - \nu^2)}$, where E and ν are, respectively, Young's modulus and the Poisson ratio of the plate material, the fluid density ρ_P, and the undisturbed flow velocity U. As shown in Fig. 1, W and V are, respectively, the transverse and longitudinal displacements of the plate. F_L and F_D are the aero/hydro-dynamic loads acting on the plate in the transverse and longitudinal directions, respectively. S is the distance of a material point on the plate from the origin, mea-

sured along the plate centreline in a coordinate system embedded in the plate. Moreover, material damping of the Kelvin-Voigt model is considered for the plate, with the loss factor being denoted by a.
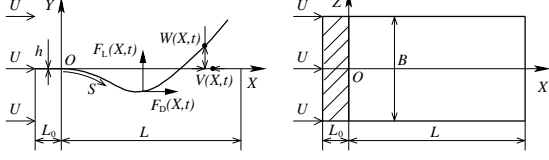

Figure 1: A cantilevered flexible in axial flow.

The equations of motion of the plate can be written in nondimensional form as (Tang and Païdoussis, 2007)

$$
\frac{1}{\mu U_{\mathrm{R}}{}^2} \left\{ \ddot{w} + \left(1 + \alpha \frac{\partial}{\partial \tau}\right) \right.
$$
$$
\times \quad \left[w'''' \left(1 + w'^2\right) + 4w'w''w''' + w''^3 \right]
$$
$$
\left. - \quad (T^\star w')' \right\} = f_{\mathrm{L}}, \tag{1}
$$

$$
v = -\frac{1}{2} \int_0^s w'^2 \, ds, \tag{2}
$$

where the overdot and the prime represent $\partial(\ )/\partial\tau$ and $\partial(\ )/\partial s$, respectively. The nondimensional tension in the plate $T^\star$ is given by

$$
T^\star = \int_s^1 (\mu U_{\mathrm{R}}{}^2 f_{\mathrm{D}} - \ddot{v}) \, ds. \tag{3}
$$

The nondimensional variables are defined by

$$
(x, y) = \frac{(X, Y)}{L}, \ (w, v) = \frac{(W, V)}{L}, \ s = \frac{S}{L},
$$
$$
\tau = \frac{t}{\sqrt{\rho_{\mathrm{P}} h L^4 / D}}, \ \alpha = \frac{a}{\sqrt{\rho_{\mathrm{P}} h L^4 / D}},
$$
$$
f^\star = f \sqrt{\rho_{\mathrm{P}} h L^4 / D}, \ l_0 = \frac{L_0}{L},
$$
$$
f_{\mathrm{L}} = \frac{F_{\mathrm{L}}}{\rho_{\mathrm{F}} U^2}, \ f_{\mathrm{D}} = \frac{F_{\mathrm{D}}}{\rho_{\mathrm{F}} U^2}, \tag{4}
$$

where $f^\star$ and f are, respectively, non-dimensional and dimensional vibration frequencies. Moreover, the mass ratio μ and the reduced flow velocity U_{R} are, respectively, defined by

$$
\mu = \frac{\rho_{\mathrm{F}} L}{\rho_{\mathrm{P}} h}, \quad U_{\mathrm{R}} = U L \sqrt{\frac{\rho_{\mathrm{P}} h}{D}}. \tag{5}
$$

In Eqs. (1) and (3), the aero/hydro-dynamic loads are calculated using the unsteady lumped

vortex model (Tang and Païdoussis, 2007). On each individual panel, the pressure difference across the plate Δp is first computed and then decomposed into the *lift* f_{L} and the *drag* f_{D}. That is

$$
f_{\mathrm{L}i} = \Delta p_i \cos \alpha_i, \quad f_{\mathrm{D}i} = \Delta p_i \sin \alpha_i + C_{\mathrm{D}}, \tag{6}
$$

where α_i is the incidence angle of the ith panel. An additional drag coefficient C_{D}, assuming a uniform distribution over the whole length of the plate, may be considered in f_{D} to account for the viscous effects of the fluid flow.

It follows from Eq. (1) that the nondimensional power $P_{\mathrm{F}i}^\star$ of the work done by the transverse fluid load $f_{\mathrm{L}i}$ on the ith panel, in the sense of per unit length along the spanwise dimension of the plate, can be calculated from

$$
P_{\mathrm{F}i}^\star = [f_{\mathrm{L}i} \Delta s] \, \dot{w}(s_i); \tag{7}
$$

and the nondimensional *accumulated* work $W_{\mathrm{F}i}^\star$ on the ith panel from

$$
W_{\mathrm{F}i}^\star = \int_0^\tau [f_{\mathrm{L}} \Delta s] \, \dot{w}(s_i) \, d\tau. \tag{8}
$$

Therefore, over the whole length of the plate, the nondimensional total power $\widehat{P}_{\mathrm{F}}^\star$ and the nondimensional *accumulated* total work $\widehat{W}_{\mathrm{F}}^\star$ can, respectively, be calculated by

$$
\widehat{P}_{\mathrm{F}}^\star = \sum_{i=1}^N P_{\mathrm{F}i}^\star, \qquad \widehat{W}_{\mathrm{F}}^\star = \sum_{i=1}^N W_{\mathrm{F}i}^\star, \tag{9}
$$

where N is the number of panels considered in the aero/hydro-dynamic model.

It should be noted that the total work done by the fluid load f_{L}, i.e., $\widehat{W}_{\mathrm{F}}^\star$, is the time integral of the power $\widehat{P}_{\mathrm{F}}^\star$. When the plate flutters, $\widehat{P}_{\mathrm{F}}^\star$ also oscillates about zero, as shown in Fig. 2(a); that is, in a cycle of the vibration of the plate, f_{L} does both positive work (the energy transferred from the fluid flow to the plate) and negative work (the energy transferred from the plate to the fluid flow). Since $\widehat{P}_{\mathrm{F}}^\star$ is oscillating, the plot of $\widehat{W}_{\mathrm{F}}^\star$ versus time is not smooth, as one can see in Fig. 2(b). The oscillating $\widehat{P}_{\mathrm{F}}^\star$ may be evaluated in terms of the time-averaged power $\overline{P}_{\mathrm{F}}^\star$, for example, which is the time-averaged power in a cycle of vibration of the system. In this paper, as illustrated in the inset of Fig. 2(b), we conveniently use the slope of the $\widehat{W}_{\mathrm{F}}^\star$ versus time plot, in terms of the line connecting the local maxima (or the

local minima), to calculate $\overline{P}_F^\star$. Moreover, according to the nondimensionalization scheme defined in Eq. (4), the dimensional time-averaged power $\overline{P}_F$ can be calculated by

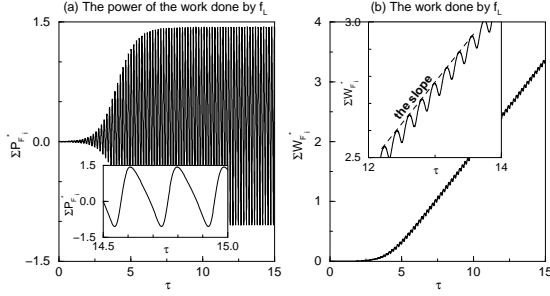$$\overline{P}_F = \rho_F U^2 \sqrt{\frac{D}{\rho_P h}} \overline{P}_F^\star. \tag{10}$$

Figure 2: The work done by the fluid load f_L and the associated power. The parameters of the system are: $\mu = 0.2$, $U_R = 10.95$, $l_0 = 0.01$, $\alpha = 0.004$ and $C_D = 0$.

3. ENERGY TRANSFER AT VARIOUS LOCATIONS OF THE PLATE

It has been shown by Tang and Païdoussis (2007) that the vibration modes of a cantilevered flexible plate in axial flow are determined by the mass ratio μ of the system. Additionally, it has been found that points at different locations along the length of the plate do not oscillate in phase (as some parts of the plate move upwards, other parts move downwards). Therefore, it is of interest to examine the energy transfer between the plate and the fluid flow at various locations along the plate for various cases of μ.

As shown in Fig. 3 for a specific system with parameters given in the figure caption, the energy transfer at various locations is not the same: energy is pumped from the fluid flow into the plate (positive slope of the $W_{Fi}^\star$ versus time plot) at some locations; while it is transferred from the plate to the fluid flow (negative slope of the $W_{Fi}^\star$ versus time plot) at other locations. In particular, $W_{Fi}^\star$ is positive at points $s_i = 0.025$ through $s_i = 0.675$; while it is negative at points $s_i = 0.750$ through $s_i = 1$. Note that in this case, the total work done by the fluid load f_L, i.e., the sum of all $W_{Fi}^\star$ along the whole length of the plate, $\widehat{W}_F^\star = \sum_{i=1}^N W_{Fi}^\star$, is positive, as shown in Fig. 3(d). The important finding is that, as

energy is pumped into the plate at the upstream section of the plate, it is transferred from the plate to the fluid flow at the downstream section.
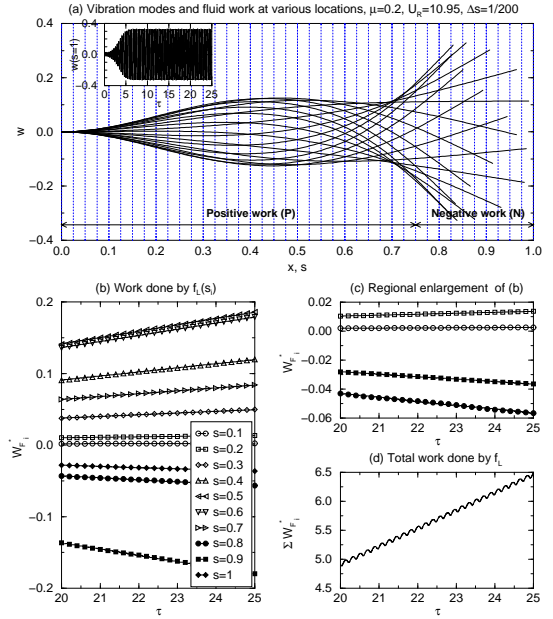
Figure 3: The energy exchange between the cantilevered flexible plate and the surrounding fluid flow along the length of the plate. The system parameters used are: $\mu = 0.2$, $U_R = 10.95 (= 1.103 U_{Rc})$, $l_0 = 0.01$, $\alpha = 0.004$ and $C_D = 0$. Note that, $N = 200$ panels are used in the numerical simulation. The energy transfer at 40 locations (every 5 panels) is recorded and the results at 10 locations (every 20 panels) are presented.

The distribution of the positive/negative $W_{Fi}^\star$ depends on the value of U_R. As shown in Fig. 4, for the case with a smaller reduced flow velocity $U_R = 10 = 1.008 U_{Rc}$ (the other parameters, especially the mass ratio μ, are the same as those of the case shown in Fig. 3), of which $\widehat{W}_F^\star$ is still positive, $W_{Fi}^\star$ is negative at points $s_i = 0.025$ through $s_i = 0.175$, positive in the range $0.2 \leq s_i \leq 0.75$ and negative at points $0.775 \leq s_i \leq 1$; note that the energy is still transferred from the plate to the fluid flow at the downstream section of the plate.

The distribution of the positive/negative $W_{Fi}^\star$ is also examined for various systems with different values of μ, as shown in Fig. 5. It should be mentioned that different values of U_R are used for individual cases of μ for the purpose of obtaining flutter motions; as shown in Table 1, for each case of μ, U_R is so chosen that it is about 10% above the corresponding critical point U_{Rc}. It
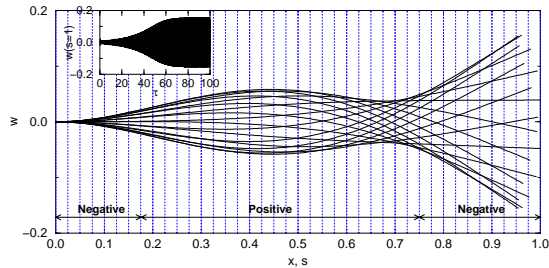
Figure 4: The positive/negative work done by the fluid load f_L at various locations along the length of the plate. The parameters of the system are: $\mu = 0.2$, $U_R = 10$, $l_0 = 0.01$, $\alpha = 0.004$ and $C_D = 0$. Note that, $N = 200$ panels are used in the numerical simulation. The energy transfer at 40 locations (every 5 panels) is recorded.

can be seen in Fig. 5 that the distribution of the positive/negative $W_{Fi}^{\star}$ depends on μ. When μ is large, say $\mu = 2$ or $\mu = 5$, higher modes become important in the dynamics of the system (Tang and Païdoussis, 2007), and the distribution of positive/negative $W_{Fi}^{\star}$ has a complicated pattern. However, when $\mu = 20$, it seems that the pattern of the distribution of positive/negative $W_{Fi}^{\star}$ does not have as many alternations in sign as the cases $\mu = 2$ and $\mu = 5$. Finally, one can see in Fig. 5 that, no matter what values of μ and U_R are used, the energy is transferred from the plate to the fluid flow at the most downstream section of the plate.

Table 1: The values of U_R used in the examination of energy transfer of various systems with different values of μ (see Fig. 5)

μ	U_{Rc}	U_R	$(U_R - U_{Rc})/U_{Rc}$
0.01	37.08	40.62	9.55%
0.5	6.9	7.48	8.45%
0.5	6.9	7.75	12.26%
2	10.78	11.83	9.76%
5	10.51	11.4	8.47%
20	8.71	9.49	8.17%

4. THE FLUTTER-MILL

It has been shown that, over the whole length of the plate and in the time-averaged sense, energy is indeed pumped into the plate from the fluid flow when flutter takes place; we can therefore utilize the energy extracted from the fluid flow to do useful work; for example, as shown in Fig. 6 in the design of a flutter-mill to generate electricity.
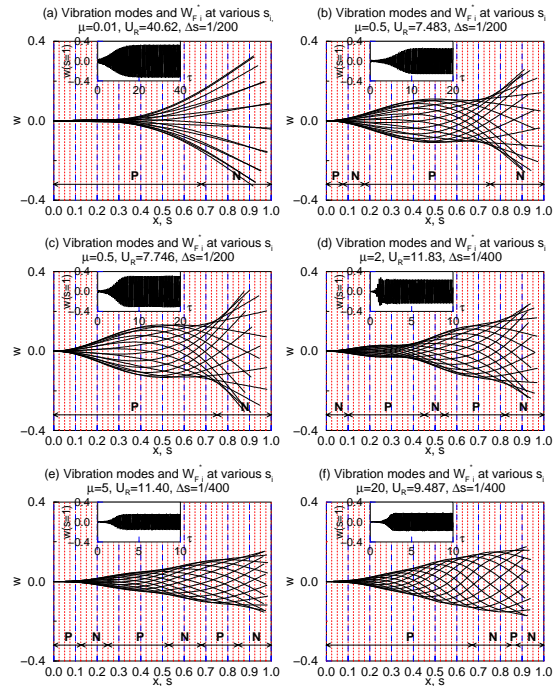

Figure 5: When flutter takes place, the positive/negative (P/N) work done by the fluid load f_L at various locations along the length of the plate. The other parameters of the system are: $l_0 = 0.01$, $\alpha = 0.004$ and $C_D = 0$. Note that, the number of panels $N = 200$ is used for the cases $\mu = 0.01$ and $\mu = 0.5$; while, for the other cases $\mu = 2$, $\mu = 5$ and $\mu = 20$, $N = 400$ is used. The energy transfers at 40 locations (every 5 panels in the case of $N = 200$ and every 10 panels when $N = 400$) are recorded.

As illustrated in Fig. 6(a), a plate made of flexible material with embedded conductors is placed between two parallel magnetic panels. When flutter takes place, the motion of each conductor in the magnetic field generates an electric potential difference between its upstream and downstream ends; and the wiring scheme shown in Fig. 6(b) ensures the formation of a closed circuit to supply electrical power to the load, say a rechargeable battery cell. The rigid bars and the additional spring supports shown in Fig. 6 are taken into consideration to make the design more realistic and/or to improve the performance of the device, for example to reduce the flutter threshold. The influence of an additional spring support or concentrated mass (i.e., the rigid bar) on the system dynamics will be studied in another paper.

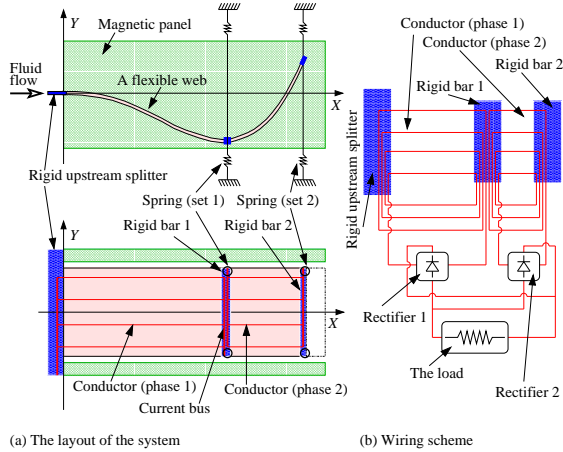As quite a few of parameters are involved in the dynamics of cantilevered flexible plates in ax-

Figure 6: The conceptual design of a flutter-mill.

Table 2: Dimensional parameters of flutter-mill

Parameters	$\mu = 0.5$	$\mu = 0.2$
ρ_F (kg/m^3) (air)	1.226	1.226
ρ_P (kg/m^3) (Al)	2840	2840
L (m)	0.58	0.232
h (m)	0.0005	0.0005

ial flow (Tang and Païdoussis, 2007) as well as in the energy transfer between the plate and the surrounding fluid flow, a starting point should be chosen for the conceptual design. We first notice that, at different sections along the plate, the energy transfer may be from the fluid flow to the plate or *vice versa*. Therefore, the conductors embedded in the flexible plate should be correspondingly arranged in several sections, or say phases. Too many phases of conductor arrangement lead to difficulties in the design of the wiring scheme and the rectifier. To this end, in the light of the vibration modes of the system with various values of mass ratio (see Fig. 12 of Tang and Païdoussis (2007), also Figs. 3–5 of the present paper), we consider the system with the mass ratio $\mu < 1$, for which the plate vibrates in the second beam mode; hence, only two phases of conductor arrangement are necessary.

In the present paper, we primarily consider two cases: $\mu = 0.5$ and $\mu = 0.2$. In the conceptual design of the flutter-mill, dimensional parameters may allow one to evaluate the performance of the device in a more direct manner; to this end, we consider a plate made of aluminium in axial air flow. The reason of considering a metallic plate is that (metal) conductors are supposed to be embedded in the plate, otherwise made of a very flexible material; the properties of this *composite* plate would be largely determined by those of the conductors. The parameters of the two systems with $\mu = 0.5$ and $\mu = 0.2$ are, respectively, listed in Table 2.

As shown in Figs. 7 and 8, preliminary calculations of the power extraction from the fluid flow demonstrate that the proposed flutter-mill is very promising for generation of electrical power.

In particular, consider a design with a mass ratio $\mu = 0.5$ and plate width $B = 0.2\,\mathrm{m}$; the device is compact, with overall dimensions length $\times$ width $\times$ height $= 0.58\,\mathrm{m} \times 0.2\,\mathrm{m} \times 0.58\,\mathrm{m}$, where the height is considered as twice the allowed maximum flutter amplitude (i.e., half of the length of the flexible plate). Such a system can be expected to extract 10 Watt power (at $U = 12\,\mathrm{m/s}$ or $43.2\,\mathrm{km/h}$) from the wind; and, if only 10% of the extracted wind energy is ultimately converted to the electrical power, an output of 1 Watt is guaranteed. Higher power output can be expected from the system with $\mu = 0.2$, which has a even smaller overall dimension as $0.232\,\mathrm{m} \times 0.2\,\mathrm{m} \times 0.232\,\mathrm{m}$ and works at higher flow velocities. Approximately, when $\mu = 0.2$, the power extraction is as high as $\overline{P}_\mathrm{F} = 1\,\mathrm{kW/m}$ at $U = 40\,\mathrm{m/s}$ or $144\,\mathrm{km/h}$.

We can compare the performance of the flutter-mill to a real HAWT, specifically the Three-Blade Stall Regulated Turbine studied by Burton et al. (2001), in terms of electrical power output, as shown in Fig. 9. The HAWT has a disk area $227\,\mathrm{m}^2$ and the data for electrical power output is collected at the rotational speed 44 rpm. In order to make a comparison, we suppose that the flutter-mill has the same wind receiving area as the HAWT ($227\,\mathrm{m}^2$) and accordingly calculate the effective width B of the plate. Moreover, in the calculation of electrical power output, we assume that only 10% of the energy captured by the plate is ultimately converted to electrical power; the other 90% is consumed by the plate for sustaining the flutter motions. It can be seen in Fig. 9 that when $\mu = 0.5$, the flutter-mill works at the lower part of wind speed range of the HAWT; however, the electrical power output of the flutter-mill is not as high as that of the HAWT (about 10%). When it is designed with $\mu = 0.2$, the flutter-mill works at high wind speed beyond the normal working condition of the HAWT, but a very high electrical power output can be expected. Therefore, it is possible to design a flutter-mill with a mass ratio between $\mu = 0.2$ and $\mu = 0.5$ to achieve an output capacity comparable to the real HAWT and to operate in the same range of wind speed as the HAWT.
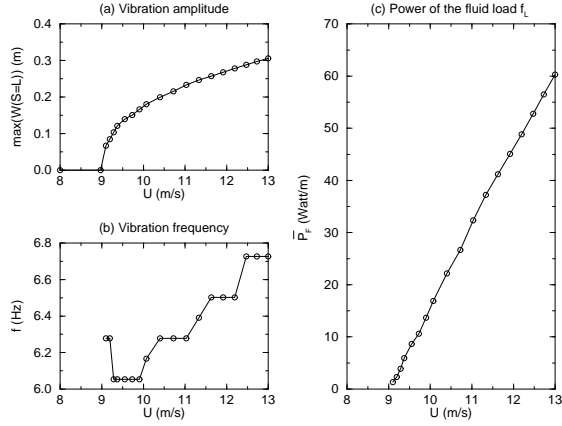
Figure 7: The dynamics of the system with $\mu = 0.5$ and the time-averaged power $\overline{P}_F$ of the fluid load f_L. The other parameters of the system are: $l_0 = 0.01$, $\alpha = 0.004$ and $C_D = 0$.

Figure 8: The dynamics of the system with $\mu = 0.2$ and the time-averaged power $\overline{P}_F$ of the fluid load f_L. The other parameters of the system are: $l_0 = 0.01$, $\alpha = 0.004$ and $C_D = 0$.

5. CONCLUSIONS

Cantilevered flexible plates in axial flow lose stability through flutter at sufficiently high flow velocity. In the present paper, the energy transfer between the plate and the surrounding fluid flow is studied. Based on the energy analysis, a new energy-harvesting device utilizing the self-induced vibrations of a cantilevered thin flexible plate in axial flow is proposed. The performance of the flutter-mill is preliminarily evaluated, and key system parameters are determined according to the dynamics of the system. The power output capacity of flutter-mills, with two typical cases of system parameters, is compared to a real HAWT. It is demonstrated that the design of a flutter-mill with high performance and compact size is very promising.

6. ACKNOWLEDGMENT

Figure 9: The performance of the flutter-mill as compared to a real HAWT, i.e., the Three-blade Stall Regulated Turbine studied by Burton et al. (2001).

7. REFERENCES

Burton, T., Sharpe, D., Jenkins, N., Bossanyi, E., 2001. *Wind Energy: Handbook*. John Wiley & Sons, Inc.: New York.

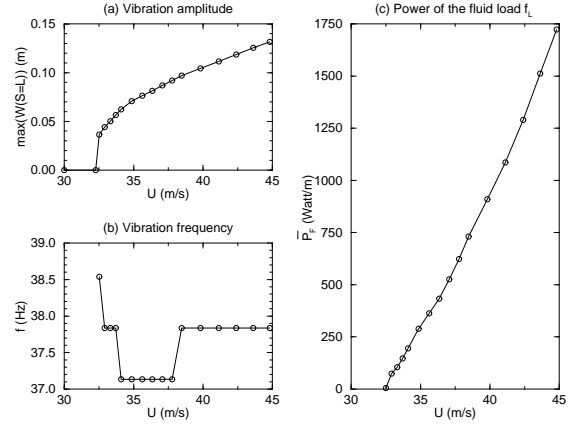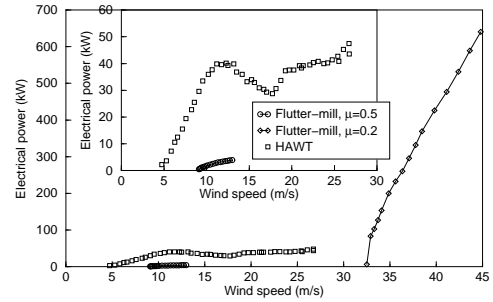Lee, A., 2004, Extraction of energy from flowing fluids. In *Canadian Patent* No. 2266632.

Matsumoto, M., Honmachi, Y., Okubo, K., Ito, Y., 2006, Fundamental study on the efficiency of power generation system by use of the flutter instability. In *Proceedings of PVP2006-ICPVT-11* No. 93773.

McKinney, W., DeLaurier, J.D., 1981, The wingmill: an oscillating-wing windmill. In *Journal of Energy* **5**: 109-115.

Tang, L., Païdoussis, M.P., 2007, On the instability and the post-critical behavior of two-dimensional cantilevered flexible plates in axial flow. In *Journal of Sound and Vibration* **305**: 97-115.